Hybridization of Nonlinear and Mixed-Integer Linear Programming for Aircraft Separation With Trajectory Recovery

Jérémy Omer and Jean-Loup Farges

***Abstract*—The approach presented in this paper aims at finding a solution to the problem of conflict-free motion planning for multiple aircraft on the same flight level with trajectory recovery. One contribution of this work is to develop three consistent models, i.e., from a continuous-time representation to a discrete-time linear approximation. Each of these models guarantees separation at all times and trajectory recovery, but they are not equally difficult to solve. A new hybrid algorithm is thus developed to use the optimal solution of a mixed-integer linear program as a starting point when solving a nonlinear formulation of the problem. The significance of this process is that it always finds a solution when the linear model is feasible while still taking into account the nonlinear nature of the problem. A test bed containing numerous data sets is then generated from three virtual scenarios. A comparative analysis with three different initializations of nonlinear optimization validates the efficiency of the hybrid method.**

***Index Terms*—Air traffic control (ATC), conflict resolution, mixed-integer linear programming (MILP), nonlinear programming (NLP), optimal control.**

I. Introduction

AIR TRAFFIC control (ATC) is the last stage of the current air traffic management (ATM) system. It aims at monitoring current air traffic in real time. If necessary, ATC is responsible for requesting changes in the trajectories of aircraft to maintain a reference horizontal separation of 5 NM or a vertical reference separation of 1000 ft. ATC is presently performed by human operators. Air space is divided in geographical volumes, and each volume is supervised by a pair of ATC officers (ATCOs). ATCOs are able to fulfill their task in the current network, but the air space is congested, and many flights are delayed to keep air traffic density below manageable thresholds. The European research project on ATM, i.e., Single European Sky ATM Research, points to automation as a key feature for the improvement of ATC [1].

A *conflict* between two aircraft is detected when both the horizontal and the vertical reference separation distances are not respected. Automated ATC systems usually aim at finding the trajectories of a set of aircraft such that a cost function is minimized and no pairwise conflict is detected in the next 10–15 min. In classical studies, trajectories are obtained by a sequence of maneuvers that each aircraft has to execute. These maneuvers may be classified into three categories, namely, turns or *heading changes*, modifications of speed norm or *speed changes*, and vertical maneuvers.

The generic problem of collision avoidance is intrinsically difficult because it is nonconvex. Even with no constraint on motion dynamics, finding collision-free paths for rectangular objects was proved to be PSPACE-hard [2]. In addition, mechanic and aerodynamic laws governing aircraft motion are very complex, and finding the optimal trajectory of one aircraft is challenging in itself [3].

Conflict-free motion planning for aircraft has been the subject of many studies. See the remarkable review on automated ATC in [4] to get an extensive view on the problem. The state of the art given as follows illustrates some promising approaches.

Kirwan and Flynn [5] and Farley and Erzberger [6] remain in a framework that is very close to current operations. Efficient maneuvers are identified for pairwise conflicts, and a heuristic search determines which action should be carried out. Such a process cannot guarantee that conflict-free trajectories are found; thus, in [5], ATCOs are allowed to handle the situation in case of failure. Theoretical studies of the pairwise conflict with no bound on velocity [7] and with constant velocity [8] were carried out in the *optimal control* framework. Optimal trajectories were determined for this simple case and applied to the general case through a genetic algorithm [7] and a heuristic procedure [8].

Without prejudging what a good maneuver should be, the problem may be simplified by allowing only one initial modification of speed vectors [9]–[11]. Mixed-integer linear programming (MILP) may then be solved to find conflict-free trajectories with speed modifications only, with heading modifications only [9], or with both maneuvers [10]. In [11] the 3-D problem is treated by using mixed-integer nonlinear programming (NLP). These approaches have to be included in a *receding horizon* procedure, which iteratively solves the problem every t min to find the best speed vector at each time step. Unfortunately, each optimal solution is based on the assumption that only one speed modification will be carried out. Although, for instance, [10] takes into account the recovery of the initial trajectory in the objective function through an

Manuscript received April 23, 2012; revised September 19, 2012 and January 18, 2013; accepted March 29, 2013. Date of publication April 26, 2013; date of current version August 28, 2013. The Associate Editor for this paper was J.-P. B. Clarke.

The authors are with the Office National d'Etudes et Recherches Aérospatiales (Onera)—The French Aerospace Lab, 31000 Toulouse, France (e-mail: jeremy.omer@gmail.com; jean-loup.farges@onera.fr).

Color versions of one or more of the figures in this paper are available online at http://ieeexplore.ieee.org.

Digital Object Identifier 10.1109/TITS.2013.2257758

estimate of the additional distance traveled, these models do not explicitly include decision variables describing the maneuvers leading to recovery.

Alonso-Ayuso *et al.* [12] described MILP with multiple speed and altitude changes. They gave an interesting analysis of tightening techniques that were implemented to solve their model more quickly. Richards and How [13] and Menon *et al.* [14] presented complete models of the problem with multiple speed modifications. In [13], MILP was solved after making the separation constraints linear, whereas in [14], original constraints were kept, and NLP was solved. The strength of an MILP formulation is that its resolution converges to a globally optimal solution, but it only gives the optimum of an approximate model. On the other hand, nonlinear optimization may take into account the real constraints, but there is no guarantee that it will lead to a feasible solution, and when it does, it only converges to a local optimum. Global optimization techniques were developed to establish proofs of convergence when solving a nonconvex NLP. For instance, deterministic algorithms for global optimization may involve some *divide* and *conquer* technique to explore the entire admissible space by sequentially solving subproblems after partitioning the original space [15]. They usually require great computational effort and may not be suited for this particular problem.

The main contributions of this paper deal with modeling and algorithmic issues. As opposed to previous works involving an MILP formulation, a consistent evolution of the constraints, i.e., from their natural continuous-time representation to their discrete-time linear approximation, is presented. This rational approach allows for an analysis of the discretization process and gives more insight on the differences between the different models. Additionally, constraints imposing trajectory recovery after the maneuvers are explicitly included. A hybrid algorithm is also developed to cope with the difficulties encountered when solving the nonlinear model. It takes advantage of the optimality of the MILP solutions to find a good starting point for the resolution of NLP, which considers the real geometry of the nonlinear constraints.

The basic problem formulation in continuous time is presented in Section II. Section III gives an NLP formulation to solve the problem numerically. An initialization process through MILP is given in Section IV, and improvements to this model, which is developed with a view to reducing computation time, are described in Section V. Finally, Section VI describes the benchmark on which the models are tested and reports associated results.

II. Continuous-Time Formulation

A. Working Hypotheses

Several hypotheses are first stated to clarify the exact ATC problem that is tackled in this paper.

Centralized Planning: ATC is a centralized decision system. It is responsible for and has authority on the whole controlled air space. The automated system presented here follows this conception of ATC. All aircraft trajectories are planned at the same time, hence taking every possible interference between aircraft into account.

Planar Motion: Current traffic is organized in horizontal layers, which are called *flight levels*, meeting the standard vertical separation. The traffic considered in this paper is limited to aircraft flying at a high altitude, whose flight level is supposed to be stabilized. This portion of air traffic is also called *en-route traffic*. Maneuvers consisting in changing flight level to avoid a conflict are not popular, being uneconomic, uncomfortable for passengers, and hard to monitor for ATCOs. This study then deals with planar motion planning of multiple aircraft flying on the same flight level.

4-D Contracts: With a view to improving traffic predictability, several projects consider a trajectory-based ATM in which an aircraft would have to meet 4-D waypoints along its flight [1], [16]. We define the *reference trajectory* of an aircraft as a planned trajectory that would satisfy every 4-D waypoint. It is also assumed that each aircraft would follow its reference trajectory if there is no other aircraft to avoid. To allow for such 4-D contracts, the problem solved here constrains the aircraft to recover their reference trajectories by the end of the conflict resolution time window.

Optimal Trajectories: This problem aims at finding cost-minimizing conflict-free motion planning. The cost of a solution is assumed to be proportional to aircraft accelerations along their trajectories.

B. Kinodynamic Planning

The motion planning problem deals with a set of aircraft $\mathcal{A}$, between which separation has to be maintained during time interval $[0, T]$. The point mass aircraft model described in [14] is commonly accepted to represent dynamical effects in civil aviation. Due to its complexity, there is a high risk that planning trajectories of several interfering aircraft with such a model would require too much computational effort. In the case of planar motion, a good approximation of the aircraft point mass model dynamics is derived in [8]. The state of an aircraft i at time t is represented by vector $\mathbf{p}_i(t)$, whose Cartesian coordinates are $(p_{i,x}(t), p_{i,y}(t))$, and by its heading angle $\chi_i(t)$. The dynamics of the system to be controlled is given by, $\forall i \in \mathcal{A}$, $\forall t \in [0, T]$

$$\begin{pmatrix} \dot{p}_{i,x}(t) \\ \dot{p}_{i,y}(t) \end{pmatrix} = V_i(t) \times \begin{pmatrix} \cos\chi_i(t) \\ \sin\chi_i(t) \end{pmatrix}$$

$$\dot{\chi}_i(t) = \omega_i(t)$$

where functions $t \mapsto \omega_i(t)$ and $t \mapsto V_i(t)$ are the control variables of the dynamical system. $V_i(t)$ is the horizontal velocity at t; $\omega_i(t)$ has the dimensions of an angular speed and is called *yaw rate*. In this model, [8] assumes that an autopilot is able to track the horizontal velocity and the yaw rate by adjusting aircraft commands properly. This assumption is guaranteed by bounds on V and ω, i.e., $\forall i \in \mathcal{A}$, $\forall t \in [0, T]$

$$\underline{V_i} \leq V_i(t) \leq \overline{V_i}$$

$$|\omega_i(t)| \leq \frac{\rho}{V_i}$$

where ρ is a constant issued from usual operational practice in terms of bank angles. As margins on speed are narrow in en-route traffic, the bound on yaw rate is approximated by constant factor $\rho/(V_i^{\mathrm{ref}})$, where V_i^{ref} is the constant velocity of aircraft i on its reference trajectory.

In our approach, since polar coordinates of speed (V, χ) cannot be made linear, it is more relevant to favor a dynamical system expressed in Cartesian coordinates, i.e., $\forall i \in \mathcal{A}$, $\forall t \in [0, T]$

$$\begin{pmatrix} \dot{p}_{i,x}(t) \\ \dot{p}_{i,y}(t) \\ \dot{v}_{i,x}(t) \\ \dot{v}_{i,y}(t) \end{pmatrix} = \begin{pmatrix} v_{i,x}(t) \\ v_{i,y}(t) \\ u_{i,x}(t) \\ u_{i,y}(t) \end{pmatrix} \tag{1}$$

where $(v_{i,x}(t), v_{i,y}(t))$ and $(u_{i,x}(t), u_{i,y}(t))$ are the Cartesian coordinates of speed and acceleration at time t; the associated vectors are $\mathbf{v}_i(t)$ and $\mathbf{u}_i(t)$. The control variables are the two coordinates of acceleration. Bounds on the horizontal velocity are maintained as in [8] by, $\forall i \in \mathcal{A}$, $\forall t \in [0, T]$

$$\underline{V_i}^2 \le \|\mathbf{v}_i(t)\|^2 \le \overline{V_i}^2 \tag{2}$$

where $\|\cdot\|$ is the Euclidean norm. The constraint on yaw rate is conserved by a bound on the norm of acceleration. By formulating the derivatives of $v_{i,x}^2(t)$ and $v_{i,y}^2(t)$ in the polar coordinates, we get

$$\|\mathbf{u}_i(t)\|^2 = \left(\dot{V}_i(t)\right)^2 + V_i^2(t)\omega_i^2(t).$$

Hence, $|\omega| \le (\rho/V)$ is guaranteed if, $\forall i \in \mathcal{A}$, $\forall t \in [0, T]$

$$\|\mathbf{u}_i(t)\|^2 \le \rho^2 \left(= \overline{U_i}^2\right). \tag{3}$$

C. Separation Constraints

In this paper, two aircraft i and j are said to be in *potential conflict* when the minimum distance between their reference trajectories is inferior to an arbitrary danger threshold (20–50 NM, depending on their relative direction). Let $\mathcal{C}$ be the set of pairs of aircraft in potential conflict. There is no conflict within time window $[0, T]$ if and only if the following separation constraint is respected, i.e., $\forall (i, j) \in \mathcal{C}$, $\forall t \in [0, T]$

$$\|\mathbf{p}_j(t) - \mathbf{p}_i(t)\|^2 \ge D^2 \tag{4}$$

where D is the horizontal reference separation distance.

A realistic formulation of the problem shall also account for the existence of prohibited areas, or *segregated areas*, in air space. Some portions of the air space are indeed reserved, at least on a temporary basis, for military use. Rectangular motionless obstacles were already considered in [13]. The constraint in [13] is extended to any polygonal obstacle o that is delimited by a set of edges $\mathcal{E}_o$. Each polygon is then described by a set of affine inequalities $a_e x + b_e y + c_e \le 0$, $e \in \mathcal{E}_o$. Let $\mathcal{O}$ be the set of obstacles; to avoid $o \in \mathcal{O}$, the position (p_x, p_y) of an aircraft has to verify at least one of the inequalities $a_e p_x + b_e p_y + c_e \ge 0$, $e \in \mathcal{E}_o$. Avoidance of all obstacles is thus guaranteed if and only if, $\forall o \in \mathcal{O}$, $\forall i \in \mathcal{A}$, $\forall t \in [0, T]$

$$\max_{e \in \mathcal{E}_o} \left(a_e p_{i,x}(t) + b_e p_{i,y}(t) + c_e\right) \ge 0. \tag{5}$$

D. Complete Problem

In addition to the constraints previously stated, we have the following.

- Initial position and speed of aircraft i, i.e., $\mathbf{p}_i^{\mathrm{ini}}$ and $\mathbf{v}_i^{\mathrm{ini}}$, represent its present state and are supposed to be known.
- Each aircraft i has to recover its reference position and speed $\mathbf{p}_i^T$ and $\mathbf{v}_i^T$ by time T.
- Optimal motion planning minimizes the norm of the control variables over $[0, T]$.

Tracking of the original plans is ensured by recovering reference positions and speeds at the end of the time interval. Most models found in the literature include a term ensuring the minimization of flight time in their criterion [8], [11], [13], [14]. Due to trajectory recovery, such a term would be redundant here. Instead, we chose to minimize the norm of the control variables with a view to performing as smooth and small variations of speed and heading as possible. This criterion, or an equivalent criterion, is used in conjunction with other criteria by several authors [9], [13], [14]. Other objective functions based on fuel consumption or on deviation from reference trajectory could also be considered in a similar model.

The overall model may be formulated as a Bolza problem, i.e.,

$$\mathcal{P} = \begin{cases} \min \quad z = \sum_{i \in \mathcal{A}} \left(\int_0^T \|\mathbf{u}_i(t)\|\, dt\right) \\ \text{subject to constraints } (1)-(5), \text{ and} \\ (\mathbf{p_i}(0), \mathbf{v}_i(0)) = \left(\mathbf{p}_i^{\mathrm{ini}}, \mathbf{v}_i^{\mathrm{ini}}\right), \ \forall i \in \mathcal{A} \\ (\mathbf{p}_i(T), \mathbf{v}_i(T)) = \left(\mathbf{p}_i^T, \mathbf{v}_i^T\right), \ \forall i \in \mathcal{A} \\ \mathbf{p}_i(t), \mathbf{v}_i(t), \mathbf{u}_i(t) \in \mathbb{R}^2, \ \forall t \in [0, T], \forall i \in \mathcal{A}. \end{cases} \tag{6}$$

Partial solutions of $\mathcal{P}$ were found in [8], but they only exhibited portions of trajectories that are optimal for pairwise conflicts. No complete analytical solution of $\mathcal{P}$ was found yet.

III. Discrete-Time Nonlinear Model

To solve $\mathcal{P}$ numerically, the time window is discretized into a sequence of $K+1$ instants $0 = t_0 < t_1 < \cdots < t_K = T$. Converting the continuous-time problem $\mathcal{P}$ into a discrete-time problem is called *direct transcription* (see [17] for an overview of numerical resolution in optimal control). The model derived through direct transcription is NLP. As far as modeling is concerned, two major difficulties arise during transcription. The differential equations (1) and the criterion of (6) have to be numerically integrated, and the constraints have to be respected for all $t \in [0, T]$. In many studies on automated ATC involving numerical resolution, these issues are simplified by considering piecewise linear trajectories (e.g., [9], [10], and [12]). These models consider that speed changes are instantaneous, which is only acceptable if maneuvers are initiated a long time before conflict [18]. After studying the error made by assuming that speed changes are instantaneous, Paielli stated that speed changes at constant acceleration are a much more acceptable option [18]. The numerical resolution of $\mathcal{P}$ was then simplified by assuming that acceleration is a piecewise constant function whose discontinuities correspond to the reception of control orders. If sequence $\mathcal{T}$ is chosen so that new orders may only be issued at an instant $t \in t_0, \ldots, t_K$, acceleration is constant on each interval $[t_k, t_{k+1}]$. In the rest of this paper, the following notations are used.

- $\mathcal{T} = \{t_k\}_{k\in\{0,\ldots,K\}}$ and $\mathcal{T}^- = \{t_k\}_{k\in\{0,\ldots,K-1\}}$.
- $\mathcal{T}$ is partitioned according to a constant time step Δ : $\forall t_k \in \mathcal{T}^-, t_{k+1} - t_k = \Delta$.
- The value that function f takes at an instant $t_k \in \mathcal{T}$ is denoted as $f^k = f(t_k)$.

A. Numerical Integration

Numerical integration of differential equations is commonly performed by a *collocation method* that approximates the solution by piecewise continuous functions such as polynomials of a chosen maximum order. In this particular case, it is assumed that acceleration is constant on each subinterval $[t_k, t_{k+1}]$. Differential equations (1) are then easy to solve exactly. Transcription of (1) leads to the exact expression, i.e.,

$$\mathbf{p}_i^{k+1} = \mathbf{p}_i^k + \Delta \times \mathbf{v}_i^k + \frac{\Delta^2}{2}\mathbf{u}_i^k,\ \forall i \in \mathcal{A}, \forall t_k \in \mathcal{T}^- \quad (7a)$$

$$\mathbf{v}_i^{k+1} = \mathbf{v}_i^k + \Delta \times \mathbf{u}_i^k,\ \forall i \in \mathcal{A}, \forall t_k \in \mathcal{T}^-. \quad (7b)$$

Acceleration being constant on each subinterval $[t_k, t_{k+1}]$, the criterion of $\mathcal{P}$ also has an exact expression in the discrete-time model, i.e.,

$$z_{\mathrm{NL}} = \sum_{i\in\mathcal{A}} \left(\sum_{k=0}^{K-1} \Delta \times \left\| \mathbf{u}_i^k \right\| \right).$$

B. State and Control Constraints

State constraints of the continuous-time problem $\mathcal{P}$ are given by upper bounds on velocity (2) and acceleration (3), separation constraints (4), and obstacle constraints (5). They have to be respected at any instant of the time horizon.

1) Bounds on Speed and Acceleration: In this model, acceleration of aircraft i is piecewise constant, and speed is piecewise linear. The two-variable function $(x, y) \to x^2 + y^2$ is convex; therefore, upper bounds on speed and acceleration are convex constraints. Hence, it is sufficient to verify these constraints at each time step, i.e., $\forall i \in \mathcal{A}$

$$\left\|\mathbf{v}_i^k\right\|^2 \le \overline{V_i}^2,\ \forall t_k \in \mathcal{T} \text{ and } \left\|\mathbf{u}_i^k\right\|^2 \le \overline{U_i}^2,\ \forall t_k \in \mathcal{T}^-. \quad (8)$$

Lower bounds on speed lead to concave constraints; however, as far as ATC is concerned, these bounds are set to keep speed in a small range, i.e., around nominal speed. For instance, Paielli [18] stated that speed decreases of more than 40 kt are often considered excessive. As this value remains a lot higher than the minimum speed induced by performance limitations, small violations of these constraints between two time steps may be accepted. Lower bound constraints are thus verified at each time step only, i.e.,

$$\left\|\mathbf{v}_i^k\right\|^2 \ge \underline{V_i}^2,\ \forall i \in \mathcal{A}, \forall t_k \in \mathcal{T}. \quad (9)$$

On the other hand, separation constraints (4) and obstacle constraints (5) do not tolerate any violation.

2) Discrete Verification of Separation Constraints: Let $(i, j) \in \mathcal{C}$ and $\mathbf{R}_i$ be the moving frame centered on i. Relative state variables of j in $\mathbf{R}_i$ are denoted with double indexes i, j, e.g., the relative position is denoted as $\mathbf{p}_{i,j} = \mathbf{p}_j - \mathbf{p}_i$. A geometric representation, in frame $\mathbf{R}_i$, of the separation constraint for (i, j) is given in Fig. 1. The constraint delimits a circular forbidden area $\mathbf{C}_i$ in the solution space for state variable $\mathbf{p}_{i,j}$. Fig. 1 shows that the separation distance might be respected at t_k and t_{k+1} while not being respected inside interval $[t_k, t_{k+1}]$.

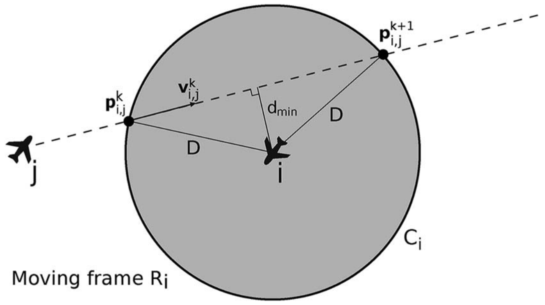

Fig. 1. Concavity of separation constraints and illustration of the worst case.

It is important to get an idea of the error made when only checking separation constraints on discrete-time space. The order of magnitude of this error is obtained by studying a simple example where relative speed is assumed to be constant, i.e., $\mathbf{v}_{i,j}(t) = \mathbf{v}_{i,j}^k$, $\forall t \in [t_k, t_{k+1}]$. In that case, the worst situation happens when both $\|\mathbf{p}_{i,j}^k\| = D$ and $\|\mathbf{p}_{i,j}^{k+1}\| = D$ (see Fig. 1). The minimum distance $\underline{d}_{i,j}^k$ between i and j is then reached at time t when the Cartesian product of $\mathbf{p}_{i,j}(t)$ and $\mathbf{v}_{i,j}^k$ vanishes. Basic geometrical considerations lead to $t = t_k + (\Delta/2)$ and

$$\left(\underline{d}_{i,j}^k\right)^2 = D^2 - \left(\frac{\Delta}{2}\left\|\mathbf{v}_{i,j}^k\right\|\right)^2.$$

Notice that this worst case often happens as it is the objective of optimization to find the shortest path. An extra margin D_m should then be added to D to ensure that i and j are always separated by the proper distance, with

$$(D + D_m)^2 = D^2 + \left(\frac{\Delta}{2}\left\|\mathbf{v}_{i,j}^k\right\|\right)^2.$$

A numerical example with $D = 5$ NM, $\Delta = 1$ min, and $\|\mathbf{v}_{i,j}^k\| = 500$ kt results in an additional margin $D_m = 4.71$ NM, which would be highly inefficient. As a consequence, it is important to find a constraint that guarantees separation at every instant.

3) Valid Separation Constraints: Due to the hypothesis of constant acceleration, the distance between aircraft i and j at time $t_k + \tau$, $\tau \in [0, \Delta]$ is

$$d_{i,j}(t_k + \tau) = \left\| \mathbf{p}_{i,j}^k + \tau \mathbf{v}_{i,j}^k + \frac{\tau^2}{2}\mathbf{u}_{i,j}^k \right\|.$$

To find $\tau_{i,j}^k$ so that minimum distance $d_{i,j}^{\min}$ is equal to $d_{i,j}(t_k + \tau_{i,j}^k)$, it is necessary to find the roots of the polynomial

$$d^{\dot{2}}_{i,j}(t_k + \tau) = 2\left\langle \mathbf{p}_{i,j}^k | \mathbf{v}_{i,j}^k \right\rangle + 2\left(\left\langle \mathbf{p}_{i,j}^k | \mathbf{u}_{i,j}^k \right\rangle + \left\langle \mathbf{v}_{i,j}^k | \mathbf{v}_{i,j}^k \right\rangle\right)\tau$$
$$+3\left\langle \mathbf{v}_{i,j}^k | \mathbf{u}_{i,j}^k \right\rangle \tau^2 + \left\langle \mathbf{u}_{i,j}^k | \mathbf{u}_{i,j}^k \right\rangle \tau^3$$

where $\langle \cdot | \cdot \rangle$ is the Euclidean scalar product. Separation constraints thus involve the roots of a third-degree polynomial. The number of distinct real roots of this polynomial depends on the sign of the discriminant. If included in the model, these constraints would have to be written as disjunctions of highly nonlinear expressions. Large-scale problems with such constraints are usually too difficult to be efficiently solved.

Let us first consider the case where velocity is constant on subinterval $[t_k, t_{k+1}]$, i.e., $\mathbf{u}_{i,j}(t_k + \tau) = 0$ for $\tau \in [0, \Delta]$. If velocity is constant, the only root of $\dot{d^2_{i,j}}(t_k + \tau)$ is easily obtained as

$$\tau^k_{i,j} = -\frac{\langle \mathbf{v}^k_{i,j} | \mathbf{p}^k_{i,j} \rangle}{\langle \mathbf{v}^k_{i,j} | \mathbf{v}^k_{i,j} \rangle}.$$

The minimum distance between i and j on $[t_k, t_{k+1}]$ is reached at

$$\bar{t}^k_{i,j} = \begin{cases} t_k, & \text{if } \tau^k_{i,j} \leq 0 \\ t_{k+1}, & \text{if } \tau^k_{i,j} \geq t_{k+1} \\ t_k + \tau^k_{i,j}, & \text{otherwise.} \end{cases} \tag{10}$$

The separation constraint between i and j on $[t_k, t_{k+1}]$ is then

$$d^2_{i,j}\left(t_k + \max\left(0, \min\left(\Delta, \tau^k_{i,j}\right)\right)\right) \geq D^2.$$

The error made by assuming that speed is constant is now calculated. Let $\tilde{\mathbf{p}}_{i,j}(t)$ be an approximate position with constant speed and $\tilde{\mathbf{v}}^k_{i,j}$ be the associated constant speed on $[t_k, t_{k+1}]$. $\tilde{\mathbf{p}}^k_{i,j}$ and $\tilde{\mathbf{v}}^k_{i,j}$ are chosen so that $\tilde{\mathbf{p}}_{i,j}(t_k) = \mathbf{p}^k_{i,j}$ and $\tilde{\mathbf{p}}_{i,j}(t_{k+1}) = \mathbf{p}^{k+1}_{i,j}$, i.e.,

$$\tilde{\mathbf{v}}^k_{i,j} = \mathbf{v}^k_{i,j} + \frac{\Delta}{2}\mathbf{u}^k_{i,j}.$$

The error made when approaching $\mathbf{p}_{i,j}$ with $\tilde{\mathbf{p}}_{i,j}$ on $[t_k, t_{k+1}]$ is given by

$$\|\mathbf{p}_{i,j}(t_k + \tau) - \tilde{\mathbf{p}}_{i,j}(t_k + \tau)\| = \frac{1}{2}\tau(\Delta - \tau)\left\|\mathbf{u}^k_{i,j}\right\|$$

which is maximal for $\tau = \Delta/2$. As a consequence, separation of all pairs of aircraft in potential conflict is guaranteed by, $\forall (i,j) \in \mathcal{C}, \forall t_k \in \mathcal{T}^-$

$$\left\|\tilde{\mathbf{p}}_{i,j}\left(\bar{t}^k_{i,j}\right)\right\|^2 \geq \left(D + \frac{\Delta^2}{8}\left\|\mathbf{u}^k_{i,j}\right\|\right)^2 \tag{11}$$

where $\bar{t}^k_{i,j}$ is calculated as in (10).

Typical values of $\overline{U}$ result in error term $(\Delta/8)\|\mathbf{u}^k_{i,j}\| \leq 1$ NM. Directly adding the error term in the constraint leads to an interesting behavior in the overall traffic: Aircraft mostly modify their speed before and after potential conflicts so that the error term has no impact when close to the conflict. Conflict resolution is mostly done in this manner today. ATCOs send orders several minutes before a detected conflict, and clearance to recover initial trajectories is only sent once the conflict is sure to be solved.

4) Obstacle Constraints: Polygonal constraints are problematic for aircraft i when closest edge e for which $a_e p_{i,x} + b_e p_{i,y} + c_e \geq 0$ changes. Aircraft could be outside the obstacle at time t_k and t_{k+1} while crossing it in the meantime. A conservative option is chosen to avoid such a situation. For all aircraft i and all subintervals $[t_k, t_{k+1}]$, it is required that at least one edge stays with its constraint verified for the whole time interval. Similar calculations lead to constraints, $\forall i \in \mathcal{A}$, $\forall t_k \in \mathcal{T}$

$$\max_{e \in \mathcal{E}_o}\left(\min\left(a_e p^k_{i,x} + b_e p^k_{i,y} + c_e - m_e,\right.\right.$$
$$\left.\left. a_e p^{k+1}_{i,x} + b_e p^{k+1}_{i,y} + c_e - m_e\right)\right) \geq 0 \tag{12}$$

with m_e as an additional margin, taking into account nonconstant speed. m_e depends on the angle between obstacle edges and is less than 1 NM for typical values of Δ, $\overline{V}$, and $\overline{U}$.

C. Summary of the NLP

The complete nonlinear model $\mathcal{P}_{\text{NL}}$ is summarized as follows:

$$\mathcal{P}_{\text{NL}} = \begin{cases} \min \quad z_{\text{NL}} = \sum\limits_{i \in \mathcal{A}} \left(\sum\limits_{k=0}^{K-1} \Delta \left\|\mathbf{u}^k_i\right\| \right) \\ \text{subject to constraints } (7){-}(12), \text{ and} \\ \forall i \in \mathcal{A}: \\ \quad \left(\mathbf{p_i}^0, \mathbf{v}^0_i, \mathbf{p}^K_i, \mathbf{v}^K_i\right) = \left(\mathbf{p}^{\text{ini}}_i, \mathbf{v}^{\text{ini}}_i, \mathbf{p}^T_i, \mathbf{v}^T_i\right) \\ \mathbf{p}^k_i, \mathbf{v}^k_i \in \mathbb{R}^2, \ \forall i \in \mathcal{A}, \forall t_k \in \mathcal{T} \\ \mathbf{u}^k_i \in \mathbb{R}^2, \ \forall i \in \mathcal{A}, \forall t_k \in \mathcal{T}^-. \end{cases}$$

It is well known that the solution of a nonconvex NLP depends on the initial point from which it is started. Several global optimization techniques rely on stochastic generation of multiple initial points before running the NLP solver on each point [19]. Although it cannot prove the optimality of a given solution, stochastic global optimization offers an asymptotic convergence guarantee in some probabilistic sense. These approaches thus constitute a faster alternative to deterministic global optimization. On the other hand, such a *multistart* technique still requires that NLP is solved several times to perform well, which may already be far too costly for large conflict-free planning of multiple aircraft trajectories. The option that was preferred in this paper focused on generating a unique good starting point. $\mathcal{P}_{\text{NL}}$ is then approximated by MILP for which a global optimum may be found in reasonable time for most operational cases.

IV. Mixed-Integer Linear Formulation

A linear program (LP) is an optimization problem formulated as the minimization of a linear criterion subject to a set of linear constraints on continuous variables. An LP is a very popular framework in optimization because some algorithms, such as the Dantzig simplex [20] or the interior-point algorithm [21], proved to be very efficient. Several works on conflict-free trajectory planning proposed a linear model for the automation of ATC [9], [13], [22], [23], for the motion of virtual humans [24], or for the general case of multiple robots [25].

Modeling this problem as an LP is not natural due to the nonconvex separation constraints. The goal may be achieved

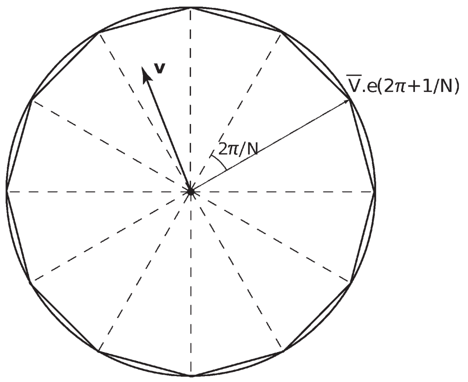

Fig. 2. Approximation of upper bounds with chords.

by making strong assumptions that are not consistent with the search of a solution close to the global optimum of $\mathcal{P}_{\mathrm{NL}}$. The model is very close to an LP when deviations are plainly forbidden, i.e., $\omega = 0$ [9], when a set of decisions is done before resolution, as in [22], or under rules of reciprocal collision avoidance [24]. As the approached model aims at finding an initial solution for NLP resolution, the same assumptions must be done in both formulations. Discussions in the following sections show that $\mathcal{P}_{\mathrm{NL}}$ may be approximated with a linear criterion and linear constraints, but separation constraints involve continuous and binary variables, hence leading to MILP.

A. Convex Constraints on Speed and Acceleration

Upper bounds on acceleration and velocity are convex, but they are quadratic. These constraints may be interpreted geometrically as circles, inside of which speed and acceleration vectors have to lie. As in [13] and [22], an upper bound is approximated by N chords equally spread on the circle (cf. Fig. 2).

Property 1: The relative error made by approximating a circle with N equally spread chords is $1 - \cos(\pi/N)$.

Proof: The maximum error is reached on the middle of each chord. Basic geometry considerations lead to the result. ■

Letting $\theta \in [0, 2\pi]$, vector $\mathbf{e}(\theta)$ is defined as $\mathbf{e}(\theta) = (\cos\,\theta, \sin\,\theta)$. For any vector $\mathbf{v}$, the set of equations

$$\left\langle \mathbf{v} \middle| \mathbf{e}\left(\frac{(2n-1)\pi}{N}\right)\right\rangle \le \overline{V}\cos\left(\frac{\pi}{N}\right), \qquad n = 1, \dots, N$$

is a conservative linear approximation of constraint $\|\mathbf{v}\| \le \overline{V}$ with maximum relative error $1 - \cos(\pi/N)$. Although it might result in a great number of additional constraints, they only involve real variables, which are easy to handle when compared with binary variables.

This formulation does not allow to compute the nonlinear criterion, but a set of intermediate variables $\overline{u}_i^k$ might be used to get a good approximation of $\|\mathbf{u}_i^k\|$. The following approximate constraints on acceleration are then considered:

$$\begin{aligned}\left\langle \mathbf{u}_i^k \middle| \mathbf{e}\left(\frac{(2n-1)\pi}{N}\right)\right\rangle &\le \overline{u}_i^k\cos\left(\frac{\pi}{N}\right), \qquad \forall i, k, n\\ 0 \le \overline{u}_i^k &\le \overline{U}_i, \quad \forall i, k.\end{aligned} \tag{13}$$

Instead of being directly bounded by $\overline{U}_i$, the norm of acceleration is bounded by $\overline{u}_i^k$, which is bounded by $\overline{U}_i$. If $\overline{u}_i^k$ is minimized, it gets as close as possible to the norm of acceleration. It is thus equivalent to minimize $\|\mathbf{u}_i^k\|$ and $\overline{u}_i^k$. This leads to a linear form of the criterion

$$z_{\mathrm{MIL}} = \sum_{i \in \mathcal{A}} \left(\sum_{k=0}^{K-1} \Delta \times \overline{u}_i^k \right).$$

Regarding velocity, it is convenient to save a great number of constraints by considering that not every direction is efficient or even reachable for short-term conflict avoidance. Denote ψ_i^k as the angle between $\mathbf{v}_i^k$ and the speed vector on reference trajectory at time t_k. It was empirically observed during tests on a reduced version of the benchmark described in Section VI that ψ_i^k remained in the range of $[-(\pi/4), (\pi/4)]$. Upper bounds on velocity are then respected if $2Q + 1$ constraints are set in the range of $[-(\pi/4), (\pi/4)]$ around the reference speed. Thus, $\forall i \in \mathcal{A}, t_k \in \mathcal{T}, q = 0, \dots, 2Q$

$$\left\langle \mathbf{v}_i^k \middle| \mathbf{e}\left(\frac{(q-Q)\pi}{4Q} + \psi_{i,k}^{\mathrm{ref}}\right)\right\rangle \le \overline{V}_i \cos\left(\frac{\pi}{8Q}\right) \tag{14}$$

where $\psi_{i,k}^{\mathrm{ref}}$ is the direction of reference speed on $[t_k, t_{k+1}]$.

B. Nonconvex Constraints

Approximating $\mathcal{P}_{\mathrm{NL}}$ with a linear model actually consists in forming a disjunction of convex problems. Let us focus on a potential conflict between two aircraft i and j. Once represented in moving frame $\mathbf{R}_i$, the separation constraint excludes separation circle $\mathbf{C}_i$ (see Fig. 1). As the half-planes delimited by the straight lines tangent to $\mathbf{C}_i$ are the biggest convex sets excluding $\mathbf{C}_i$, it is adequate to approximate separation constraints by disjunctions of such half-planes.

The difficulty due to the quadratic evolution of position with respect to time is handled as for the nonlinear case. Conflicts are solved for aircraft with constant speed $\tilde{\mathbf{v}}_{i,j}^k = \mathbf{v}_{i,j}^k + (\Delta/2)\mathbf{u}_{i,j}^k$, and the error made is compensated by adding a term to the separation distance. The modified separation distance is

$$D_{i,j}^k = D + \frac{\Delta^2}{8}\left(\overline{u}_i^k + \overline{u}_j^k\right).$$

If speed is constant on $[t_k, t_{k+1}]$, the motion of aircraft j in $\mathbf{R}_i$ is a straight line. Separation is thus guaranteed on $[t_k, t_{k+1}]$ if j is on the separating side of the same tangent at both t_k and t_{k+1}, as is represented in Fig. 3. The constraint is conservative because it may force an aircraft to move away from the reference trajectory, although separation is already performed. This is, however, essential to maintain proper separation at every moment. Eventually, the separation constraint is approximated by a set $\mathcal{S}$ of tangents, above one of which j has to be at both t_k and t_{k+1} to avoid conflict during $[t_k, t_{k+1}]$. Such disjunction is modeled with linear constraints by using binary variables. Optimization decides which tangent maintains separation between i and j on $[t_k, t_{k+1}]$ by setting the values of binary variables $\delta_{i,j,s}^k$, $s \in \mathcal{S}$, such that $\delta_{i,j,s}^k = 1$ if j is on the

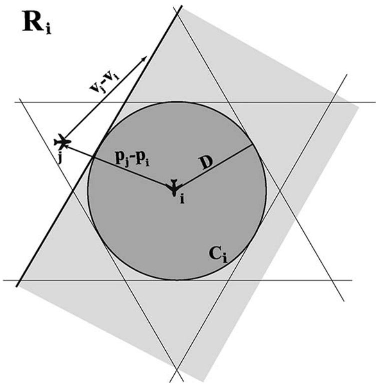

Fig. 3. Approximation of the separation circle with tangents.

side of tangent s that does not include $\mathbf{C}_i$ during $[t_k, t_{k+1}]$, and $\delta^k_{ij,s} = 0$ otherwise. Let θ_s, $s \in \mathcal{S}$, be such that s is tangent to $\mathbf{C}_i$ at point $D \times \mathbf{e}(\theta_s)$. Separation on $[t_k, t_{k+1}]$ is formulated as, $\forall t_k \in \mathcal{T}^-$, $\forall (i,j) \in \mathcal{C}$

$$\left\langle \mathbf{p}^k_{i,j} | \mathbf{e}(\theta_s) \right\rangle \geq D^k_{i,j} - M\left(1 - \delta^k_{i,j,s}\right), \qquad \forall s \in \mathcal{S} \quad (15)$$

$$\left\langle \mathbf{p}^{k+1}_{i,j} | \mathbf{e}(\theta_s) \right\rangle \geq D^k_{i,j} - M\left(1 - \delta^k_{i,j,s}\right), \quad \forall s \in \mathcal{S} \quad (16)$$

$$\sum_{s \in S} \delta^k_{i,j,s} = 1 \quad (17)$$

$$\delta^k_{i,j,s} \in \{0,1\}, \quad \forall s \in \mathcal{S}. \quad (18)$$

Positive constant M is chosen big enough to ensure that constraints (15) and (16) are redundant for any relative position if $\delta^k_{i,j,s} = 0$. Constraints (17) make sure that at least one tangent is separating i and j on $[t_k, t_{k+1}]$. This technique is commonly used to formulate disjunctive constraints in MILP. It is usually referred to as the big-M formulation.

Following a similar reasoning, avoidance of segregated areas $o \in \mathcal{O}$ is modeled with linear constraints involving binary variables $\delta^k_{i,e}$, $e \in \mathcal{E}_o$, such that aircraft i is on the side of edge e that does not include o during $[t_k, t_{k+1}]$ if $\delta^k_{i,e} = 1$, i.e., $\forall i \in \mathcal{A}$, $\forall t_k \in \mathcal{T}^-$, $\forall o \in \mathcal{O}$

$$a_e p^k_{i,x} + b_e p^k_{i,y} + c_e + m_e \geq M\left(\delta^k_{i,e} - 1\right), \forall e \in \mathcal{E}_o \quad (19)$$

$$a_e p^{k+1}_{i,x} + b_e p^{k+1}_{i,y} + c_e + m_e \geq M\left(\delta^k_{i,e} - 1\right), \forall e \in \mathcal{E}_o \quad (20)$$

$$\sum_{e \in \mathcal{E}_o} \delta^k_{i,e} = 1. \quad (21)$$

The lower bound on speed is also ensured by a disjunctive constraint. If quadratic constraint $\|\mathbf{v}\|^2 \geq \underline{V}^2$ is represented by a circle outside of which $\mathbf{v}$ has to lie, a linear approximation is obtained by considering a set of tangents instead of the chords involved in the upper bound constraints. The lower bound is thus satisfied if $\mathbf{v}$ satisfies at least one of the constraints associated with the tangents. This is formulated through constraints similar to (14) by adding a set of binary variables $\epsilon^k_{i,q}$, i.e., $\forall i \in \mathcal{A}$, $\forall t_k \in \mathcal{T}$, $\forall q \in \{0, \ldots, 2Q\}$

$$\left\langle \mathbf{v}^k_i \middle| \mathbf{e}\left(\frac{(q-Q)\pi}{4Q} + \psi^{\text{ref}}_{i,k}\right) \right\rangle \geq \underline{V}_i - M'\left(1 - \epsilon^k_{i,q}\right) \quad (22)$$

$$\sum_{q \in \{0,\ldots,2Q\}} \epsilon^k_{i,q} = 1 \quad (23)$$

$$\epsilon^k_{i,q} \in \{0,1\}. \quad (24)$$

C. Summary of the MILP

The complete MILP $\mathcal{P}_{\text{MIL}}$ is given as

$$\mathcal{P}_{\text{MIL}} = \begin{cases} \min \quad z_{\text{MIL}} = \sum_{i \in \mathcal{A}} \left(\sum_{k=0}^{K-1} \Delta \times \overline{u}^k_i\right) \\ \text{subject to constraints } (7), (13) - (14) \\ \text{and } \forall i \in \mathcal{A}: \\ \left(\mathbf{p_i}^0, \mathbf{v}^0_i, \mathbf{p}^K_i, \mathbf{v}^K_i\right) = \left(\mathbf{p}^{\text{ini}}_i, \mathbf{v}^{\text{ini}}_i, \mathbf{p}^T_i, \mathbf{v}^T_i\right) \\ \mathbf{p}^k_i, \mathbf{v}^k_i \in \mathbb{R}^2, \ \forall i \in \mathcal{A}, \forall t_k \in \mathcal{T} \\ \mathbf{u}^k_i \in \mathbb{R}^2, \overline{u}^k_i \in \mathbb{R}^+, \ \forall i \in \mathcal{A}, \forall t_k \in \mathcal{T}^- \\ \delta^k_{i,j,s} \in \{0,1\}, \ \forall (i,j) \in \mathcal{C}, \forall t_k \in \mathcal{T}^-, \forall s \in \mathcal{S} \\ \delta^k_{i,e} \in \{0,1\}, \ \forall i \in \mathcal{A}, \forall t_k \in \mathcal{T}^-, \forall e \\ \epsilon^k_{i,q} \in \{0,1\}, \ \forall i \in \mathcal{A}, \forall t_k \in \mathcal{T}, \forall q. \end{cases}$$

V. Computational Analysis and Improvements

$\mathcal{P}_{\text{MIL}}$ is a disjunction of a large number of LPs. By exploring the tree built from possible decisions with an efficient algorithm such as a *branch-and-bound* algorithm, which was first described in [26], it is possible to find the global optimum of the overall problem. At each node of the tree, a *continuous relaxation* of $\mathcal{P}_{\text{MIL}}$ is solved by fixing a set of binary variables to chosen values and by replacing constraints $\delta \in \{0,1\}$ with $\delta \in [0,1]$ for the other variables. In this framework, computation time mostly depends on three criteria:

1) the size of the continuous relaxation, given by its number of constraints and variables;
2) the number of binary variables;
3) the tightness of continuous relaxations.

The first two aspects are quantified as follows. In the following property, $|\mathcal{S}et|$ refers to the cardinal of $\mathcal{S}et$, and the total number of edges is denoted by E, i.e., $E = \sum_{o \in \mathcal{O}} |\mathcal{E}_o|$.

Property 2: $\mathcal{P}_{\text{MIL}}$ is composed of

- $7\ |\mathcal{A}| \times K$ continuous variables for position, speed, and acceleration;
- $K \times |\mathcal{S}| \times |\mathcal{C}|$ binary variables for separation and $|\mathcal{A}| \times K \times |\mathcal{O}|$ binary variables for obstacle avoidance;
- $|\mathcal{A}| \times (8 + K \times (4 + N + 4Q))$ motion constraints;
- $K \times |\mathcal{C}| \times (2|\mathcal{S}| + 2) + K \times |\mathcal{A}| \times (E + |\mathcal{O}|)$ separation and segregated area constraints.

While $|\mathcal{A}|$, $|\mathcal{C}|$, $|\mathcal{O}|$, and E are problem data, K, $|\mathcal{S}|$, N, and Q are parameters of the model. As the model has to remain accurate, the problem's size may not be decreased below an acceptable threshold. The remaining option is to make continuous relaxations much tighter by calculating good values for big-M constants in (15) and (16) and by adding valid inequalities.

A. Tightening $\mathcal{P}_{\text{MIL}}$

The choice of a good value for big-M constants in (15) and (16) depends on the pair of aircraft, the instant, and the tangent considered. This means that a set of constants $\{M^k_{i,j,s}\}$ has to be determined. Let $(i,j) \in \mathcal{C}$ and $t_k \in \mathcal{T}^-$. $M^k_{i,j,s}$ and $M^{k+1}_{i,j,s}$ need to be chosen so that any pair of reachable relative positions $\mathbf{p}^k_{i,j}$ and $\mathbf{p}^{k+1}_{i,j}$ satisfies separation constraints when $\delta^k_{i,j,s} = 0$, i.e.,

$$\left\langle \mathbf{p}^k_{i,j} | \mathbf{e}(\theta_s) \right\rangle \geq \overline{D} - M^k_{i,j,s}$$
$$\left\langle \mathbf{p}^{k+1}_{i,j} | \mathbf{e}(\theta_s) \right\rangle \geq \overline{D} - M^{k+1}_{i,j,s}.$$

where $\overline{D}$ is an upper bound of $D_{i,j}^k$. The value of $M_{i,j,s}^k$ leading to the tightest formulation of $\mathcal{P}_{\text{MIL}}$ is thus given by

$$M_{i,j,s}^k = \max_{\mathbf{p}_{i,j}^k} \left\{ \overline{D} - \left\langle \mathbf{p}_{i,j}^k | \mathbf{e}(\theta_s) \right\rangle \right\}. \tag{25}$$

Alonso-Ayuzo *et al.* gave a tight MILP formulation of conflict-free motion planning with speed and altitude maneuvers [12]. In [12], 2-D paths are fixed, and only velocity or flight level vary. It is then straightforward to calculate $\{M_{i,j,s}^k\}$ so that (25) is verified. If aircraft are allowed to change their headings, finding $\{M_{i,j,s}^k\}$ involves the resolution of a maximization problem for each $(i, j) \in \mathcal{C}$, $t_k \in \mathcal{T}$ and $s \in \mathcal{S}$, which may be long and inefficient. Instead of applying such a process, it is assumed that, in optimal trajectories, maximum deviations from reference trajectories do not exceed 10% of the total reference trajectory lengths. This assumption is reasonable considering the dynamics of aircraft and the constraints that they have to be on their reference trajectories at initial and final times. It was also verified with a comfortable margin on the experimental tests described in Section VI.

Let $\mathbf{p}_i^{\text{ref}}(t)$, $t \in [0, T]$, be the reference trajectory of i and $\mathbf{d}_i(t)$, $t \in [0, T]$, be the deviation from this trajectory, i.e., $\mathbf{p}_i(t) = \mathbf{p}_i^{\text{ref}}(t) + \mathbf{d}_i(t), \forall t \in [0, T]$. If d_i^{ref} and d_j^{ref} are the maximum deviations of i and j implied by the given assumption, it is straightforward that, $\forall t_k \in \mathcal{T}, \forall s \in \mathcal{S}$

$$\left\langle \mathbf{p}_{i,j}^k | \mathbf{e}(\theta_s) \right\rangle \leq \left\langle \mathbf{p}_{i,j}^{\text{ref}}(t_k) | \mathbf{e}(\theta_s) \right\rangle + d_i^{\text{ref}} + d_j^{\text{ref}} \tag{26}$$

$$\left\langle \mathbf{p}_{i,j}^k | \mathbf{e}(\theta_s) \right\rangle \geq \left\langle \mathbf{p}_{i,j}^{\text{ref}}(t_k) | \mathbf{e}(\theta_s) \right\rangle - d_i^{\text{ref}} - d_j^{\text{ref}}. \tag{27}$$

From (27), it comes that the solution of (25) is

$$M_{i,j,s}^k = \overline{D} - \left\langle \mathbf{p}_{i,j}^{\text{ref}}(t_k) | \mathbf{e}(\theta_s) \right\rangle + d_i^{\text{ref}} + d_j^{\text{ref}}. \tag{28}$$

Moreover, (26) implies that if there exists $s \in \mathcal{S}$ such that, for some $t_k \in \mathcal{T}$

$$\left\langle \mathbf{p}_{i,j}^{\text{ref}}(t_k) | \mathbf{e}(\theta_s) \right\rangle + d_i^{\text{ref}} + d_j^{\text{ref}} < \overline{D}$$

then the separation constraint associated with (i, j), t_k, and s may be dropped as it will not be satisfied. Similarly, (26) implies that if, for any $t_k \in \mathcal{T}$, there exists $s \in \mathcal{S}$, i.e.,

$$\left\langle \mathbf{p}_{i,j}^{\text{ref}}(t_k) | \mathbf{e}(\theta_s) \right\rangle - d_i^{\text{ref}} - d_j^{\text{ref}} \geq \overline{D}$$

then all separation constraints for conflict (i, j) and time t_k may also be dropped as separation is guaranteed to be satisfied. Through such considerations, the number of constraints and binary variables is decreased for most problems, and a much tighter formulation is obtained.

A similar approach could be applied to tighten constraints (19) and (20). Finally, the best value for constant M' that appears in constraint (22) is the sum of the lower and upper bounds on velocity.

B. Valid Inequalities

It is also possible to tighten the model by appending redundant constraints, hence reducing feasible space while keeping optimal solutions. Several improvements were added to the model by considering specific properties of the application; two such simplifications are detailed as follows.

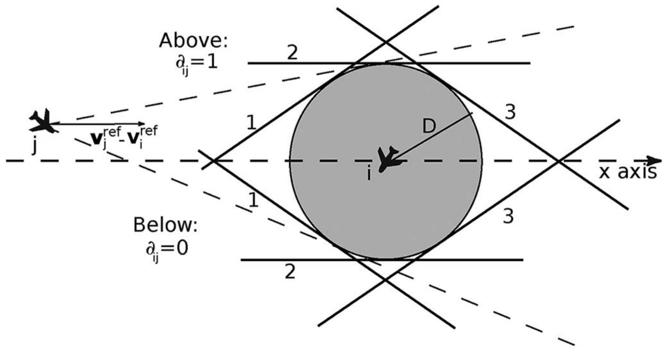

Fig. 4. Representation of valid inequalities.

Let i and j be two aircraft in potential conflict. A rotation is applied to moving frame $\mathbf{R}_i$ so that the relative speed on reference trajectories $\mathbf{v}_{i,j}^{\text{ref}}$ is collinear to the x-axis and points in the same direction, as in Fig. 5. Experimental tests conducted on pairwise conflicts showed that when i and j cross with an angle that is larger than 30°, optimal solutions never plan that j performs a u-turn in frame $\mathbf{R}_i$. Let $\mathcal{C}_{30^\circ}$ be the set of such potential conflicts. Assuming that this "no u-turn" hypothesis is valid, two sets of redundant constraints may be added to the problem. It should be observed that if the assumption is not verified, the following inequalities might prevent the solver from finding the optimal solution; however, as long as the problem remains feasible, the solution is a good candidate to initialize NLP.

It is first important to directly state in the model that, under this assumption, $\forall (i, j) \in \mathcal{C}_{30^\circ}$, j passes either below or above $\mathbf{C}_i$. This statement avoids the exploration of many useless combinations when setting the values of $\{\delta_{i,j,s}^k\}$. The expression of this redundant constraint involves one new binary variable $\delta_{i,j}$ for each potential conflict, such that $\delta_{i,j} = 1$ when j goes above $\mathbf{C}_i$ and $\delta_{i,j} = 0$ when it goes below (see Fig. 4). Letting $\mathcal{S}^+$ be the set of tangents above the circle and $\mathcal{S}^-$ be the set of tangents below the circle, the valid inequalities are formulated, i.e., $\forall (i, j) \in \mathcal{C}_{30^\circ}, \forall t_k \in \mathcal{T}$

$$\sum_{s \in \mathcal{S}^+} \delta_{i,j,s}^k \leq \delta_{i,j}, \quad \forall k \tag{29a}$$

$$\sum_{s \in \mathcal{S}^-} \delta_{i,j,s}^k \leq 1 - \delta_{i,j}, \quad \forall k. \tag{29b}$$

Under the same assumption, there also has to be a temporal progression in the choice of the separating tangents from left to right. $\mathcal{S}^+$ and $\mathcal{S}^-$ are then ordered so that $s < s' \in \mathcal{S}^+$ (or $s < s' \in \mathcal{S}^-$) implies that the binary variable associated with tangent s is set to 1 before the binary variable associated with s'. An ordering is represented by the numbering of tangents above and below the circle in Fig. 4. These constraints are then formulated as, $\forall (i, j) \in \mathcal{C}_{30^\circ}, \forall t_k \in \mathcal{T}$

$$\sum_{s \in \mathcal{S}^+} s\delta_{i,j,s}^k \leq \sum_{s \in \mathcal{S}^+} s\delta_{i,j,s}^{k+1} \tag{30a}$$

$$\sum_{s \in \mathcal{S}^-} s\delta_{i,j,s}^k \leq \sum_{s \in \mathcal{S}^-} s\delta_{i,j,s}^{k+1}. \tag{30b}$$

C. Relaxation of the Separation Constraints

When considering a large number of aircraft in potential conflict, runtime may be far over the operational requirements. It would indeed be exaggerated to spend more than 1 or 2 min looking for a resolution to conflicts that are to happen in 5–10 min. A way of tackling this issue is to add a runtime limit of, e.g., 60 s when solving the MILP and use the best feasible solution found as a candidate starting point for the optimization of $\mathcal{P}_{\mathrm{NL}}$. It is, however, not even sure that a feasible solution is found within 60 s, which is why separation constraints are relaxed by adding nonnegative slack variables penalized in the criterion. Let $\{sl_{i,j}^k\}$ be the slack variables; once relaxed, (15) and (16) become, $\forall (i,j) \in \mathcal{C}, \forall t_k \in \mathcal{T}^-$

$$\left\langle \mathbf{p}_{i,j}^k | \mathbf{e}(\theta_s) \right\rangle \geq D_{i,j}^k - M\left(1-\delta_{i,j,s}^k\right) - sl_{i,j}^k, \quad \forall s \in \mathcal{S} \quad (31)$$

$$\left\langle \mathbf{p}_{i,j}^{k+1} | \mathbf{e}(\theta_s) \right\rangle \geq D_{i,j}^k - M\left(1-\delta_{i,j,s}^k\right) - sl_{i,j}^k, \quad \forall s \in \mathcal{S} \quad (32)$$

$$sl_{i,j}^k \geq 0 \quad (33)$$

and the term $\sum_{(i,j)\in\mathcal{C}, t_k\in\mathcal{T}^-} \mu \times sl_{i,j}^k$ is added to the criterion with $\mu \gg \overline{U}$. Once separation constraints are relaxed, it is much easier to get a solution that is at least feasible with regard to every constraint but the separation constraints. By penalizing the slack variables, minimization searches solutions in which slack variables are equal to 0, which implies that the separation constraints are satisfied.

VI. Computational Experiments

A. Sensitivity to Initialization

When solving a nonconvex NLP, classical iterative algorithms only converge to a local minimum. This solution and the speed of convergence both depend on the point from which the algorithm is started. The sensitivity of the solution of $\mathcal{P}_{\mathrm{NL}}$ to initialization is first illustrated on a simple case before studying more complex scenarios.

A pairwise potential conflict between two aircraft i and j is considered, and it is assumed that all other aircraft in the vicinity are far enough to be disregarded. The problem was solved with two different initial solutions $\mathbf{T}_r^{\mathrm{ini}}$ and $\mathbf{T}_l^{\mathrm{ini}}$. On trajectories $\mathbf{T}_r^{\mathrm{ini}}$ (resp. $\mathbf{T}_l^{\mathrm{ini}}$), both aircraft make a 20° turn to the right (resp. to the left) for 2 min and then go straight until they make another 20° turn to recover their reference trajectories. Once represented in moving frame $\mathbf{R}_i$, if j follows $\mathbf{T}_r^{\mathrm{ini}}$ (resp. $\mathbf{T}_l^{\mathrm{ini}}$), it passes above (resp. below) $\mathbf{C}_i$.

$\mathcal{P}_{\mathrm{NL}}$ was solved with sparse nonlinear optimizer (SNOPT),[1] which is a software package for solving large-scale optimization problems. It uses sequential quadratic programming (SQP), which is an iterative procedure that approximates the NLP by a quadratic programming subproblem at each step. More details on SQP may be found in [27].

Solutions $\overline{\mathbf{T}}_r$ and $\overline{\mathbf{T}}_l$ are represented next to their matching initial solutions in Fig. 5. Solution $\overline{\mathbf{T}}_r$ was found to be 150% more expensive than $\overline{\mathbf{T}}_l$. Resolution kept the trajectory on the same side of $\mathbf{C}_i$ as in the initial solution, hence leading to a clearly suboptimal solution $\overline{\mathbf{T}}_r$.

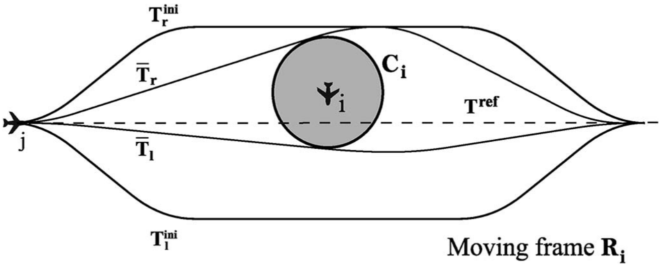
$\mathbf{T_r^{ini}}$
$\overline{\mathbf{T}}_\mathbf{r}$
$\mathbf{C_i}$
i
$\mathbf{T^{ref}}$
j
$\overline{\mathbf{T}}_\mathbf{l}$
$\mathbf{T_l^{ini}}$
Moving frame $\mathbf{R_i}$

Fig. 5. Pairwise conflict with two sets of resolutions.

B. Generation of Data Sets

To illustrate the performances of the algorithms presented in this paper, three generic data sets were chosen for their complexities and the diversity of the difficulties they offer. They focus on clusters of aircraft in potential conflict, and they were designed to cover situations ranging from what may be currently handled by ATCOs to much more complex conflicts. The aircraft of a data set are entirely described by their initial states (positions and speeds), their final goal positions, and the bounds on their speeds and accelerations. The environment is given by the equations of the edges of the polygonal segregated areas. For simplicity, all aircraft have identical performances. Parameters were chosen to represent generic performances found in the BADA database[2]: nominal velocity $V_{\mathrm{nom}} = 500$ kts, $\overline{V} = 1.05 \times V_{\mathrm{nom}}$, and $\underline{V} = 0.92 \times V_{\mathrm{nom}}$. The time interval is 10 min long and is split in ten sampling periods (i.e., $K = 10$). The number of sampling periods was set on the basis of a previous work [28], in which the effect of the number of periods was thoroughly studied on a reduced number of data sets. Although the model was not as complete as the one described in this paper, the global behavior of the algorithm was close enough to follow the conclusions that were drawn in [28] on this topic. The first type of data sets is a classical academic example in automated ATC [7], [29]. Several aircraft are initially set on a 50-NM radius circle and must reach the opposite extremity of the diameter by the end of the time range. Fig. 6(a) gives a representation of the initial situation with four aircraft. Its difficulty lies in the strong dependence between all the conflicts. It is not possible to try to solve one conflict without impacting the others. The optimal solution is known for aircraft with equal performances: All aircraft take a turn in the same direction, as if in a roundabout.

Another configuration that was considered interesting involves parallel aircraft flows intersecting perpendicularly [see Fig. 6(b)]. It aims at studying the behavior of automated ATC when several consecutive conflicts have to be handled in a very structured environment. It also illustrates specificity of air traffic because controlled air space is currently organized in routes that aircraft have to follow.

[1] http://www.sbsi-sol-optimize.com/asp/sol_product_snopt.htm

[2] BADA is the Base of Aircraft Data of EUROCONTROL. It is available online at http://www.eurocontrol.int/eec/public/standard_page/proj_BADA.html

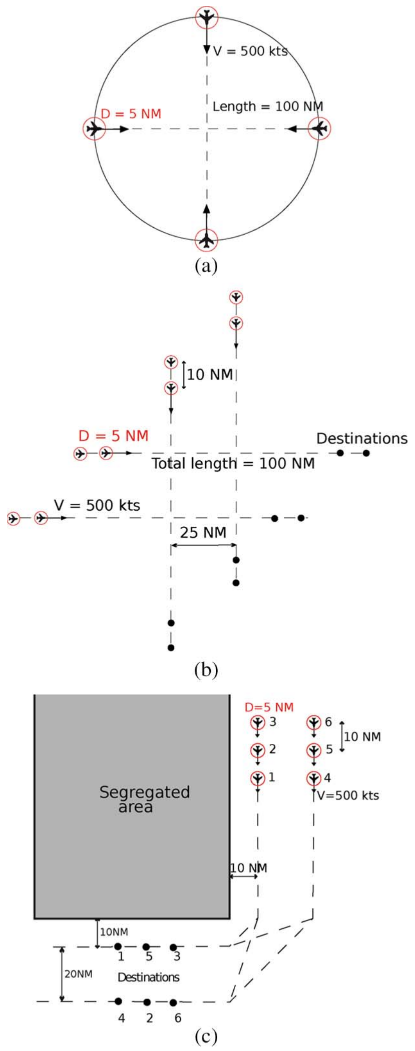

(a)

(b)

(c)

Fig. 6. Representations of the benchmark data sets. (a) Roundabout. (b) Grid. (c) Segregated area.

The third type of data sets illustrates the ability of avoiding a segregated area while managing a complex situation. The aircraft are initially organized in two parallel flows, and they have to reach final points to which the shortest path infringes on the segregated area. To make the situation more complex, the flows are mixed: Aircraft belonging to the same initial flow do not all aim at the same final route. Fig. 6(c) gives a possible implementation of this configuration with three aircraft per flow.

The three generic situations were used to generate a complete benchmark. For each scenario previously described, four configurations were chosen with increasing numbers of aircraft and conflicts. Their properties are summarized in Table I. n_v, n_b, and n_c are the numbers of variables, binary variables, and constraints in the associated tightened MILP, respectively. The high symmetry in these configurations was partly broken by adding random terms in the initial positions of the aircraft. Each aircraft was moved on its reference trajectory according to a distance that was randomly sampled from a uniform distribution on $[-3\text{ NM}, 3\text{ NM}]$. The tests were conducted on 100 randomly generated data sets for each configuration in Table I.

TABLE I
SUMMARY OF THE DATA SETS

data	scenario	$\lvert\mathcal{A}\rvert$	$\lvert\mathcal{C}\rvert$	n_v	n_b	n_c
G-01	Grid	6	15	732	125	3404
G-02	Grid	6	15	774	153	3516
G-03	Grid	8	28	1142	268	4972
G-04	Grid	12	66	1866	476	7838
R-01	Roundabout	3	3	342	51	1632
R-02	Roundabout	4	6	512	102	2308
R-03	Roundabout	5	10	746	194	3146
R-04	Roundabout	6	15	1008	303	4050
S-01	Seg. Area	4	6	928	414	3444
S-02	Seg. Area	5	10	1370	664	4860
S-03	Seg. Area	6	15	1896	977	6498
S-04	Seg. Area	7	21	2506	1346	8358

C. Computational Results

This section reports the results obtained when solving $\mathcal{P}_{\mathrm{NL}}$ for the data sets described in the preceding section. As it was observed in Section VI-A that solving $\mathcal{P}_{\mathrm{NL}}$ was sensitive to initialization, three options were considered to provide a good starting point. Such a resolution is often referred to as a *warm start*.

Solving the complete MILP, as presented in Section IV, provides the optimal solution of an approximate problem. It ensures that the solver process starts from a good point that might even be in the neighborhood of the NLP optimum in some cases. The MILP solution being feasible for $\mathcal{P}_{\mathrm{NL}}$, the current best solution of the solver is always feasible, which means that it may be stopped at any moment to return an efficient motion planning for the aircraft. This *any time* property is very useful in an application such as ATC where reactivity and robustness are important. The hybrid warm-start optimization of $\mathcal{P}_{\mathrm{NL}}$ from the solution of $\mathcal{P}_{\mathrm{MIL}}$ is denoted by $\mathcal{S}_h$. Due to the fact that waiting for the MILP to converge may take too much time, another candidate starting point was obtained by adding a time limit of 60 s when solving $\mathcal{P}_{\mathrm{MIL}}$. The separation constraints were relaxed, as described in Section V-C, to make sure that a solution is always found. This alternative process is denoted by $\mathcal{S}_h^{60}$. As they are already available without any further calculation, reference trajectories were provided as a third candidate starting point to $\mathcal{P}_{\mathrm{NL}}$ resolution. The reference trajectories satisfy every constraint but separation constraints. In the simple pairwise conflict studied in Section VI-A, this starting point also leads to the best solution. Warm-start optimization from reference trajectories is denoted by $\mathcal{S}_{\mathrm{ref}}$.

When solving $\mathcal{P}_{\mathrm{MIL}}$, the lower bounds on velocity (22)–(24) were withdrawn because the recovery of the planned positions and speeds associated with the minimization of acceleration is more likely to lead to velocities above nominal speed. A post-process routine was implemented to verify that lower bounds are satisfied and to solve $\mathcal{P}_{\mathrm{MIL}}$ again with constraints (22)–(24) if it is not the case. However, this second resolution was never needed because no violation of (22)–(24) was detected by the routine during the tests.

The values of parameters N and Q involved in the linearization of the quadratic constraints on velocity and acceleration did not impact computation time seriously, which is why they were set to rather high values, i.e., $N = 40$ and $2Q = 10$. On the other hand, computation time is very sensitive to the number

TABLE II
COMPUTATIONAL RESULTS FOR EACH ALGORITHM

data	$\%_0$	$\%_r$	$\%_h$	$\%_h^{60}$	z_0	z_r	z_M	z_h	z_M^{60}	z_h^{60}
G-01	100	100	100	100	19.3	18.3	26.2	12.9	26.2	12.9
G-02	91	100	100	100	42.4	16.3	17.2	14.3	17.2	14.3
G-03	100	100	100	100	42.1	36.4	25.0	20.2	25.1	20.2
G-04	88	99	100	99	88.3	53.1	35.4	27.4	47.7	40.8
R-01	100	100	100	100	11.6	9.8	9.9	8.9	9.9	8.9
R-02	100	100	100	100	17.5	15.6	16.3	14.1	16.3	14.1
R-03	87	88	100	100	40.6	28.1	24.9	21.5	24.9	21.5
R-04	62	89	100	100	58.8	34.6	34.9	29.6	35.4	29.8
S-01	99	99	100	100	48.9	48.4	49.0	48.4	49.0	48.4
S-02	99	99	100	100	65.4	60.5	61.2	60.5	61.2	60.5
S-03	99	97	100	100	76.5	72.6	73.7	72.6	73.7	72.6
S-04	100	99	100	100	96.3	84.9	85.9	84.8	86.1	85.0

TABLE III
COMPUTATION TIME FOR EACH ALGORITHM (SECONDS)

data	t_0	t_r	t_{NL}	t_M	t_h	t_{NL}^{60}	t_M^{60}	t_h^{60}
G-01	8	3	3	6	8	3	6	8
G-02	5	2	3	3	6	3	3	6
G-03	10	6	4	33	37	4	26	30
G-04	61	25	11	658	670	14	60	74
R-01	1	1	1	1	2	1	1	2
R-02	2	2	1	2	3	1	2	3
R-03	3	2	2	23	24	2	23	24
R-04	6	4	2	98	100	2	59	61
S-01	4	3	2	3	5	2	3	5
S-02	8	4	4	6	10	4	6	10
S-03	18	8	6	17	23	6	17	23
S-04	29	11	9	54	63	11	41	52

of separation tangents, which is why $|\mathcal{S}|$ was set to its minimal value, i.e., $S = 4$.

$\mathcal{P}_{\mathrm{MIL}}$ was solved by running commercial solver Gurobi.[3] As most MILP solvers, Gurobi explores the search tree with a branch-and-bound method and tightens the continuous relaxation by generating valid inequalities. See [30] for an overview of the current MILP solvers and the advanced techniques they employ. The implementation of the improvements described in Section V-A and B speed up the resolution of $\mathcal{P}_{\mathrm{MIL}}$ by a factor of 2–10. Most of this acceleration is due to valid inequalities. As in Section VI-A, $\mathcal{P}_{\mathrm{NL}}$ was solved with SNOPT. The default options of both solvers were used. Computations were performed on a PC Intel Xeon with a 2.80-GHz processor and 12 GB of random access memory.

Tables II and III report comparative results for the three warm starts previously introduced and for a resolution where no starting point is provided to the solver, which is denoted by $\mathcal{S}_0$. In Table II, column headers $\%_0$, $\%_r$, $\%_h$, and $\%_h^{60}$ are the percentages of data sets for which a feasible solution was found by $\mathcal{S}_0$, $\mathcal{S}_{\mathrm{ref}}$, $\mathcal{S}_h$, and $\mathcal{S}_h^{60}$, respectively. As finding a feasible solution is the primary objective, the other columns give average results over the data sets for which every method found a feasible solution. z_0, z_r, z_h, and z_h^{60} are the costs of the best solutions found by $\mathcal{S}_0$, $\mathcal{S}_{\mathrm{ref}}$, $\mathcal{S}_h$, and $\mathcal{S}_h^{60}$. The costs z_M and z_M^{60} of the initial solutions found by solving $\mathcal{P}_{\mathrm{MIL}}$ with no time limit and with a 60-s time limit were added. Through the construction of $\mathcal{P}_{\mathrm{MIL}}$, they provide an upper bound of z_h and z_h^{60} and indicate how much the resolution of $\mathcal{P}_{\mathrm{NL}}$ was able to improve this starting point. In Table III, t_0, t_r, t_h, and t_h^{60} are the elapsed times (in seconds) to find these solutions. Computation times of the hybrid algorithm, i.e., t_h and t_h^{60}, are decomposed to give insight on the proportion of time spent in the resolutions of $\mathcal{P}_{\mathrm{MIL}}$ (t_M and t_M^{60}) and $\mathcal{P}_{\mathrm{NL}}$ (t_{NL} and t_{NL}^{60}).

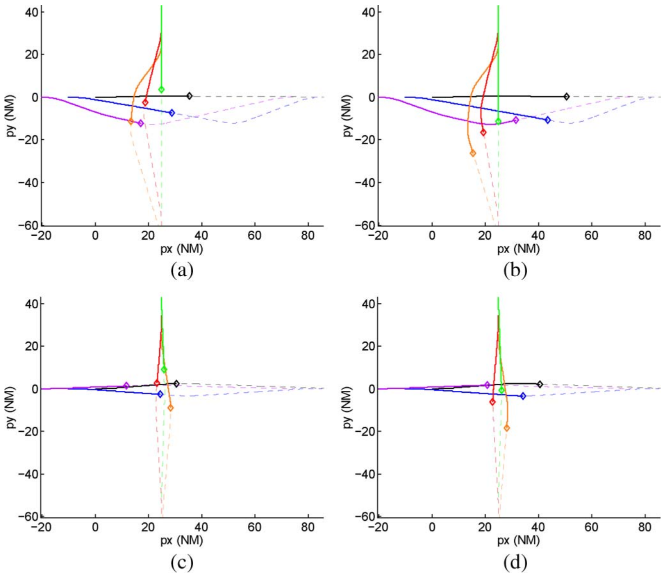

Fig. 7. (Top) Infeasible and (bottom) feasible trajectories for G-02. A specific color is assigned to each aircraft. (a) $\mathcal{S}_0$, $t = 4.5$ min. (b) $\mathcal{S}_0$, $t = 6.3$ min. (c) $\mathcal{S}_h$, $t = 4.0$ min. (d) $\mathcal{S}_h$, $t = 5.2$ min.

A first analysis of the results in Table II focuses on feasibility. The SQP algorithm implemented in SNOPT alternates between a phase where a quadratic criterion subject to a linear approximation of the constraints is solved to get the next iterate, which might not satisfy all nonlinear constraints, and an elastic phase during which feasibility is recovered with respect to a given tolerance. In most cases, an infeasible solution satisfies the linear constraint but does not meet the feasibility tolerance with respect to nonlinear constraints, although SNOPT minimized these nonlinear infeasibilities. This was the case when $\mathcal{S}_0$ or $\mathcal{S}_{\mathrm{ref}}$ did not converge to a feasible solution. The trajectories characterized by infeasible solutions thus look implementable but slightly violate either the upper bound on velocity, the separation constraints, or both. Contrary to $\mathcal{S}_0$ and $\mathcal{S}_{\mathrm{ref}}$, hybrid algorithm $\mathcal{S}_h$ was always able to find a feasible solution because the global search realized when solving $\mathcal{P}_{\mathrm{MIL}}$ was successful in providing a starting point that is feasible for $\mathcal{P}_{\mathrm{NL}}$. In this respect, it is also remarkable that $\mathcal{S}_{\mathrm{ref}}$ always performed better than $\mathcal{S}_0$. This shows that even a partially feasible solution constitutes a valuable starting point.

By focusing on the results of $\mathcal{S}_0$, it appears that it was more difficult to find a feasible solution for G-02 than for G-03, although G-03 involves more aircraft. This behavior is explained by the fact that G-02 simulates the encounter of two trails of three aircraft, whereas G-03 involves trails of two aircraft [G-03 is the scenario drawn in Fig. 6(b)]. In Fig. 7, an infeasible solution produced by $\mathcal{S}_0$ for G-02 is compared with the feasible solution produced by $\mathcal{S}_h$. The diamond symbols give the positions of the aircraft at t, and dotted lines correspond

[3] Gurobi website: http://gurobi.com

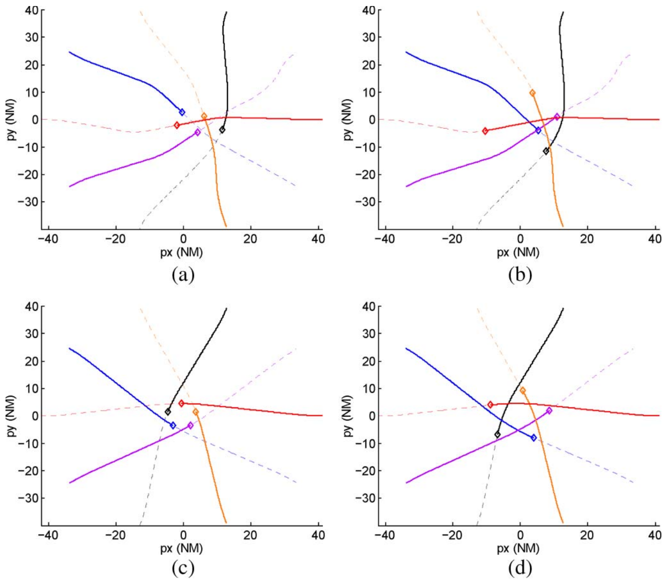

(a) (b)

(c) (d)

Fig. 8. (Top) Infeasible and (bottom) feasible trajectories for R-03. A specific color is assigned to each aircraft. (a) $\mathcal{S}_{\text{ref}}$, $t = 5$ min. (b) $\mathcal{S}_{\text{ref}}$, $t = 6$ min. (c) $\mathcal{S}_h$, $t = 5$ min. (d) $\mathcal{S}_h$, $t = 6$ min.

to the remaining parts of the trajectories. In the solution of $\mathcal{S}_0$, the whole vertical trail goes behind the horizontal trail, which results in a 2.5-NM minimum distance between the first aircraft of the vertical trail and the last aircraft of the horizontal trail. Although the solution of $\mathcal{S}_h$ is feasible and the associated trajectories look implementable, it results in a situation that ATCOs may still consider too dangerous because the aircraft of the vertical trail go between successive aircraft of the horizontal trail. To find more robust trajectories, the uncertainties should be explicitly included in the models. On the other hand, it is interesting to observe in Fig. 8 that trajectories found by $\mathcal{S}_h$ are naturally structured as in a roundabout, whereas the more costly solution found by $\mathcal{S}_{\text{ref}}$ presents no specific structure.

Solution costs also followed the same hierarchy between the models. Solutions found by $\mathcal{S}_h$ were, on average, 15% better than $\mathcal{S}_{\text{ref}}$ solutions and 32% better than $\mathcal{S}_0$. The solutions of $\mathcal{P}_{\text{MIL}}$ were already cheaper than those of $\mathcal{S}_{\text{ref}}$ and $\mathcal{S}_0$, and the resolution of $\mathcal{P}_{\text{NL}}$ improved them by an average 10%. $\mathcal{S}_{\text{ref}}$ also proved to be an efficient alternative to $\mathcal{S}_{\text{MIL}}$ in terms of cost.

Finally, the runtime of $\mathcal{S}_h$ was bigger in every case, although t_{NL} and t_{NL}^{60} are slightly smaller than t_0 and t_r. The starting point obtained by solving $\mathcal{P}_{\text{MIL}}$ accelerates the convergence of the resolution of $\mathcal{P}_{\text{NL}}$, but $\mathcal{P}_{\text{MIL}}$ is a large-scale MILP, which may be time consuming. Nevertheless, computational effort remains below 40 s for most data sets. Computation time would only be unacceptable for the biggest "grid" and "roundabout" data sets, i.e., G-04 and R-04, and could be found excessive for some S-04 data sets. The difficulties encountered when solving a "roundabout" scenario are mostly due to its highly symmetric structure, which is usually a major obstacle to combinatorial optimization. The last "grid" data set, i.e., G-04, was longer to solve because it involves many more aircraft. It is, however, important to notice that such complex situations are never met in current air traffic. Situations where six interacting aircraft are in potential conflict are exceptional, and the air space structure forbids such symmetric trajectories as in "grid" and "roundabout" scenarios. If such a situation is encountered in real traffic, the quick resolution obtained by adding a time limit of 60 s proved to be efficient as it only failed to find a feasible solution once and still provides solutions whose costs are smaller than z_0 and z_r, even if a 50% cost increase was observed for G-04.

VII. Conclusion

The objective of the approach presented in this paper is to solve the problem of conflict-free motion planning for multiple aircraft on the same flight level with trajectory recovery. One of the major advancements in this paper is a consistent approximation scheme from the natural continuous-time representation of the problem to a discrete-time linear approximation. In particular, it connects formulations that are usually independently treated in the literature. Moreover, the approximations are chosen to satisfy the requirements for separation between aircraft at all times with accurate constraints. The operational concept of a 4-D contract is also taken into account by explicitly including in the model the recovery of reference trajectories after the necessary maneuvers. The second important contribution is a hybrid algorithm in which warm-start optimization of a nonlinear model is performed from the solution of a linear approximation. This algorithm enables taking into consideration the real geometry of nonlinear constraints while guaranteeing to find a feasible solution when the linear model has one. Experimental tests were conducted on a large benchmark, including three air traffic scenarios, which is representative of several difficulties that may be encountered. These tests highlighted the positive impact of hybridization in terms of the number of feasible solutions and of the cost of these solutions. It was, however, observed that the resolution of the mixed-integer linear model could take too much time for operational implementation. A significant improvement in runtime with only a minor deterioration of the solutions was achieved by stopping this resolution after 1 min when the solver has yet to converge.

On a theoretical level, a perspective that was opened by this work deals with the development of an algorithm aiming at global optimality of the NLP by iteratively improving bounds on its criterion. Indeed, it is possible to build a linear approximation whose minimum cost is a lower bound of the optimal cost of the NLP. This approximation may be obtained by a process that is similar to the process described in this paper, except that, when linearizing quadratic constraints, chords should be replaced with tangents and, reciprocally, tangents with chords.

Our current research on the subject focused on improving the implementability of the models with the aim of integrating it in a decision support system. To meet the constraints imposed by decision makers, additional research has to be conducted on four levels. The model has some limitations, such as the fact that constraints on longitudinal and lateral accelerations are not decoupled and that the criterion does not explicitly formulate the operational cost of trajectories. More precise constraints on acceleration and a cost function based on fuel consumption are to be included in the model. Moreover, as the definition of an ideal criterion is still an open issue, other criteria such as deviation from the reference trajectory could be investigated. To extend the applicability of this automated conflict resolution to aircraft whose altitude is not stabilized, a 3-D model is under study. Uncertainties should be also explicitly added in the problem to obtain robust conflict-free motion planning. It must, however, be noted that these last two improvements give rise to much more complex problems, which may only be tractable for small instances unless some simplifying assumptions are made. Finally, the benchmark proposed here was useful in demonstrating the strengths and limits of this algorithm, but it remains too artificial. There would be a need to test this method on operational data. Full-scale real-life data sets were already collected and still have to be used as other entries of our benchmark. After addressing these issues, the solver could be implemented as a module that is activated either periodically or upon request of the controllers. It will then be possible to assess the impact of the system in an operational context.

References

[1] "SESAR definition phase, deliverable 3: The ATM target concept," SESAR Joint Undertaking, Brussels, Belgium, Tech. Rep., 2007.

[2] J. Hopcroft, J. Schwartz, and M. Shahir, "On the complexity of motion planning for multiple independent objects: PSPACE-hardness of the warehouseman's problem," *Int. J. Robot. Res.*, vol. 3, no. 4, pp. 76–88, Dec. 1984.

[3] C. R. Hargraves and S. W. Paris, "Direct trajectory optimization using nonlinear programming and collocation," *J. Guid., Control, Dyn.*, vol. 10, no. 4, pp. 338–342, Jul./Aug. 1987.

[4] J. K. Kuchar and L. C. Yang, "A review of conflict detection and resolution modeling methods," *IEEE Trans. Intell. Transp. Syst.*, vol. 1, no. 4, pp. 179–189, Dec. 2000.

[5] B. Kirwan and M. Flynn, "Identification of air traffic controller conflict resolution strategies for the CORA project," presented at the Air Traffic Management (ATM) Semin., Santa Fe, NM, USA, 2001.

[6] T. Farley and H. Erzberger, "Fast-time simulation evaluation of a conflict resolution algorithm under high air traffic demand," presented at the Air Traffic Management (ATM) Semin., Barcelona, Spain, 2007.

[7] N. Durand, J.-M. Alliot, and J. Noailles, "Automatic aircraft conflict resolution using genetic algorithms," in *Proc. Symp. Appl. Comput.*, 1996, pp. 289–298.

[8] A. Bicchi and L. Pallotino, "Optimal cooperative conflict resolution for air traffic management systems," *IEEE Trans. Intell. Transp. Syst.*, vol. 1, no. 4, pp. 221–231, Dec. 2000.

[9] L. Pallottino, E. Feron, and A. Bicchi, "Conflict resolution problems for air traffic management systems solved with mixed integer programming," *IEEE Trans. Intell. Transp. Syst.*, vol. 3, no. 1, pp. 3–11, Mar. 2002.

[10] A. Vela, S. Solak, J. Clarke, W. Singhose, E. Barnes, and E. Johnson, "Near real-time fuel-optimal en route conflict resolution," *IEEE Trans. Intell. Transp. Syst.*, vol. 11, no. 4, pp. 826–837, Dec. 2010.

[11] M. Christodoulou and S. Kodaxakis, "Automatic commercial aircraft-collision avoidance in free flight: The three-dimensional problem," *IEEE Trans. Intell. Transp. Syst.*, vol. 7, no. 2, pp. 242–249, Jun. 2006.

[12] A. Alonso-Ayuso, L. Escudero, P. Olaso, and C. Pizarro, "Conflict avoidance: 0–1 linear models for conflict detection & resolution," *TOP*, pp. 1–20, Sep. 2011, Online First Article.

[13] A. Richards and J. How, "Aircraft trajectory planning with collision avoidance using mixed integer linear programming," in *Proc. Amer. Control Conf.*, 2002, vol. 3, pp. 1936–1941.

[14] P. K. Menon, G. D. Sweriduk, and B. Sridhar, "Optimal strategies for free flight air traffic conflict resolution," *J. Guid., Control, Dyn.*, vol. 22, no. 2, pp. 202–211, Mar./Apr. 1999.

[15] P. Belotti, J. Lee, L. Liberti, F. Margot, and A. Wächter, "Branching and bounds tightening techniques for non-convex MINLP," *Optim. Methods Softw.*, vol. 24, no. 4/5, pp. 597–634, Aug. 2009.

[16] S. Guibert and L. Guichard, "4D trajectory management through contract of objectives," in *Proc. 9th Innovative Res. Workshop Exhib.*, 2010, pp. 1–8.

[17] J. T. Betts, *Practical Methods for Optimal Control Using Nonlinear Programming*. Philadelphia, PA, USA: SIAM, 2001, ser. Advances in Design and Control.

[18] R. A. Paielli, "Modeling maneuver dynamics in air traffic conflict resolution," *J. Guid., Control, Dyn.*, vol. 26, no. 3, pp. 407–415, May/Jun. 2003.

[19] C. G. E. Boender, A. H. G. Rinnooy Kan, L. Stougie, and G. T. Timmer, "Global optimization: A stochastic approach," in *Numerical Techniques for Stochastic Systems*. Amsterdam, The Netherlands: North Holland, 1980, pp. 387–394.

[20] G. Dantzig, "The general simplex method for minimizing a linear form under inequality constraints," *Pacific J. Math.*, vol. 5, no. 2, pp. 183–195, Oct. 1955.

[21] Y. Nesterov and A. Nemirovski, *Interior Point Polynomial Methods in Convex Programming*. Philadelphia, PA, USA: SIAM, 1994.

[22] W. Niedringhaus, "Stream option manager (SOM): Automated integration of aircraft separation, merging, stream management, and other air traffic control functions," *IEEE Trans. Syst., Man Cybern.*, vol. 25, no. 9, pp. 1269–1280, Sep. 1995.

[23] J. Omer and T. Chaboud, "Tactical and post-tactical air traffic control methods," in *Proc. 9th Innovative Res. Workshop Exhib.*, 2010, pp. 11–18.

[24] S. J. Guy, M. C. Lin, and D. Manocha, "Modeling collision avoidance behavior for virtual humans," in *Proc. 9th Int. Conf. Autonom. Agents Multiagent Syst.*, 2010, pp. 575–582.

[25] J. Peng and S. Akella, "Coordinating multiple robots with kinodynamic constraints along specified paths," *Int. J. Robot. Res.*, vol. 24, no. 4, pp. 295–310, Apr. 2005.

[26] R. Gomory, "Outline of an algorithm for integer solutions to linear programs," *Bull. Amer. Math. Soc.*, vol. 64, pp. 275–278, May 1958.

[27] J. Nocedal and S. Wright, *Numerical Optimization*. New York, NY, USA: Springer-Verlag, 2006, ser. Springer Series in Operations Research*, 2nd ed*.

[28] J. Omer and J.-L. Farges, "Automating air traffic control through nonlinear programming," in *Proc. ICRAT*, 2012, pp. 1–8.

[29] C. Peyronne, D. Delahaye, and L. Lapasset, "Conflict-free trajectory optimization using b-splines and genetic algorithm," in *Proc. 9th Innovative Res. Workshop Exhib.*, 2010, pp. 213–218.

[30] A. Lodi and J. T. Linderoth, "MILP software," in *Encyclopedia for Operations Research and Management Science*. Hoboken, NJ, USA: Wiley, 2011.

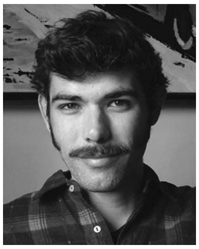

Jérémy Omer was born in Paris, France, in 1982. He received the B.S. degree in electric engineering from the École supérieure d'électricité (Supélec), Gif-sur-Yvette, France, in 2006; the M.S. degree in applied mathematics from the École Polytechnique de Montréal, Montreal, QC, Canada, in a double graduation program in 2006; and the Ph.D. degree from the Institut Supérieur de l'Aéronautique et de l'Espace, Toulouse, France, in 2013, for research conducted under the guidance of Dr. G. Verfaillie and Dr. T. Chaboud at the Office National d'Etudes et Recherches Aérospatiales (Onera)—The French Aerospace Lab.

His research interests include optimization techniques applied to logistics, robotics, and air-traffic systems.

Jean-Loup Farges was born in Clamart, France, in 1956. He received the degree in electric engineering from the École Nationale Supérieure d'Électronique, d'Électrotechnique, d'Informatique, d'Hydraulique et des Télécommunications, Toulouse, France, in 1978; the M.S. degree in automatic control from Paul Sabatier University, Toulouse; and the Ph.D. degree from the Institut Supérieur de l'Aéronautique et de l'Espace, Toulouse, in 1983.

He has since been working as a Research Scientist with the Office National d'Etudes et Recherches Aérospatiales (Onera)—The French Aerospace Lab, Toulouse. Initially, his main area of interest was road traffic control. Since 2003, his research has focused on planning and execution control for aerial vehicles and on optimization in air traffic control.